

## Prediction of a novel high-pressure phase of hydrogen peroxide

Xinyu Zhang,<sup>1</sup> Wenbo Zhao ,<sup>1</sup> Siyu Liu,<sup>1</sup> Lihua Yang,<sup>2</sup> Qing Guo,<sup>1,\*</sup> Jian Lv ,<sup>1,\*</sup> and Yanchao Wang <sup>1,3</sup>

<sup>1</sup>International Center for Computational Method and Software & State Key Laboratory of Superhard Materials, College of Physics, Jilin University, Changchun 130012, China

<sup>2</sup>Key Laboratory of Functional Materials Physics and Chemistry of the Ministry of Education, College of Physics, Jilin Normal University, Changchun 130103, China

<sup>3</sup>International Center of Future Science, Jilin University, Changchun 130012, China



(Received 11 February 2020; revised manuscript received 31 March 2020; accepted 31 March 2020; published 29 April 2020)

The binary H-O system almost exclusively exists in the form of water ice with stoichiometry of H<sub>2</sub>O in a wide range of pressure (<~5 TPa) that is one of the most abundant substances in the solar system. Hydrogen peroxide (H<sub>2</sub>O<sub>2</sub>) is only metastable at ambient condition. We herein report a stable H<sub>2</sub>O<sub>2</sub> phase at high pressure identified by first-principles calculations in combination with a swarm-intelligence structure search. The predicted H<sub>2</sub>O<sub>2</sub> compound is formed by stacking of an intriguing planar H<sub>2</sub>O<sub>2</sub> molecule different from the metastable three-dimensional isomer at ambient condition. The planarity of hydrogen peroxide molecules is expected to be caused by the steric repulsion between molecules at high pressure, which is responsible for the stability of the crystal. The phase is energetically stable in the pressure range of ~423–600 GPa. It is thus a low-pressure phase of binary H-O system with H:O stoichiometry other than 2:1 and promises to be accessible in static compression experiment.

DOI: [10.1103/PhysRevB.101.134112](https://doi.org/10.1103/PhysRevB.101.134112)

### I. INTRODUCTION

The chemical elements of hydrogen and oxygen are among the most abundant elements in the solar system [1,2]. Their binary compositions, mostly in the form of water ice with stoichiometry of H<sub>2</sub>O, are important components of giant planets under a wide range of pressure [1,3]. For example, water ice is likely in the core of Saturn and Jupiter at pressure as high as 6.4 TPa [4], and is mixed with ammonia and methane ice in Uranus and Neptune up to 800 GPa [3]. Thus, the high-pressure studies of the structure properties of water ice are of fundamental scientific interest for both condensed-matter and planetary physics.

Water ice has a very rich phase diagram. Until now, 16 crystalline phases have been identified experimentally [5,6], most of which are molecular crystals with different stacking of water molecules. At low temperature and pressure above 70 GPa, the first atomic crystal phase, ice X, emerges with symmetrical hydrogen bonds, in which the identity of water molecules is lost [7]. Static compression experiment for water has achieved pressures up to ~210 GPa [8], revealing that ice X is the highest-pressure crystalline phase thus far. However, this pressure is far below the highest pressures for water within planets. Dynamic compression techniques [9–11] can reach TPa pressures, but usually at high temperatures where the sample melts. In the context of high-pressure study of water ice, theoretical simulations have played a significant role. A number of high-pressure phases beyond ice X have been predicted through first-principles calculations

combined with advanced global structure searching methods, and the transition sequence is constantly revised up to ~50-TPa pressures [12–19]. According to the latest work, at least five high-pressure phases should exist beyond the stable field of ice X with transition sequence as follows: *Pbcm* → *Pbca* → *P3<sub>1</sub>21* → *Pcca* → *P2<sub>1</sub>/c* [12,13,16,19]. All these high-pressure phases are insulating atomic crystals with O and H atoms fourfold- and twofold coordinated with each other.

H<sub>2</sub>O is the most stable stoichiometry of H:O binary composition for a wide range of pressure, but other H:O stoichiometries could also exist. On the hydrogen-rich side of the phase diagram (H:O ratio larger than 2:1), Zhang *et al.* predicted a H<sub>4</sub>O phase to be stable relative to H + H<sub>2</sub>O above 1.4 TPa and a H<sub>3</sub>O phase to be stable relative to H<sub>2</sub>O + H<sub>4</sub>O above 14 TPa [18]. Pickard *et al.* proposed a series of hydrogen-rich phases H<sub>2+δ</sub>O with δ between 1/8 and ~5/12 at pressures of a little over 5 TPa [19]. Most recently, Huang *et al.* found a solid H<sub>3</sub>O phase stable above ~450 GPa, which transforms to a fluid metallic state at the deep interior conditions of Uranus and Neptune (>~500 GPa and ~5000 K) [20]. These stable hydrogen-rich phases are important for planetary physics, because they are likely to be formed at the core-mantle boundary of gas giant planets where H<sub>2</sub>O occurs under hydrogen-rich conditions [21]. On the oxygen-rich side of the phase diagram (H:O ratio less than 2:1), only one phase has been proposed to be stable at high pressure thus far, which is the hydrogen peroxide (H<sub>2</sub>O<sub>2</sub>) exhibiting a high-symmetry pyrite-type structure with O–O bonds and threefold-coordinated H atoms [19]. Intuitively, it is not expected to find H<sub>2</sub>O<sub>2</sub> in a H-rich condition within gas giants. However, the prediction of this phase is of particular importance, which in combination with aforementioned

\*Corresponding author: lvjian@jlu.edu.cn

H-rich phases leads to a significant conclusion of decomposition of water above 5 TPa [19].

Given the wide pressure range that the binary H-O system could exist within gas giants and the relatively simple high-pressure phase diagram on the O-rich side, it is reasonable to expect that some stable phases may be missed. Complementing the high-pressure phase diagram of the binary H-O system will inevitably advance our understanding on the structure of gas giant planets. Therefore, in this work, we performed an extensive exploration of high-pressure phase diagram of the binary H-O system on the O-rich side (H:O ratio less than 2:1) via our in-house developed swarm-intelligence CALYPSO method. Strikingly, a stable orthorhombic phase of  $\text{H}_2\text{O}_2$  is predicted to be thermodynamically stable at pressure range of about 423–600 GPa. The predicted  $\text{H}_2\text{O}_2$  is formed by stacking of intriguing planar  $\text{H}_2\text{O}_2$  molecule. It is thus far a low-pressure phase of binary H-O system with H:O stoichiometry other than 2:1 and promises to be accessible in static compression experiment using diamond-anvil cell.

## II. COMPUTATIONAL DETAILS

The search for structures of the H-O system was based on the global minimization of free-energy surfaces using *ab initio* total energy calculations and the swarm-intelligence-based CALYPSO structure prediction method [22,23]. Several techniques are included in the CALYPSO method to improve the search efficiency, e.g., space-group symmetry constraints in structural generation, a bond characterization matrix technique for fingerprinting structures, local version of the particle swarm-optimization algorithm enabling a simultaneous search in different energy funnels, etc. The key feature of this methodology is its capability of predicting the ground-state stable structure of materials with only the knowledge of chemical composition at given external conditions (for example, pressure), not relying on any prior known structural information. Its validity has been manifested by successful identification of the ground-state structures for a large number of systems [24–30].

The underlying energy calculations and structure optimizations were performed in the framework of density-functional theory using the Vienna *Ab initio* Simulation Package [31]. The projector-augmented plane-wave approach [32] was used to represent the ion-electron interaction with  $1s^2$  and  $2s^22p^4$  as valence electrons for H and O, respectively. The electron exchange-correlation functional was treated using the generalized gradient approximation proposed by Perdew, Burke, and Ernzerhof [33]. The cutoff radius of the pseudopotentials of oxygen and hydrogen are 0.58 and 0.42 Å, respectively. A cutoff energy of 1200 eV for the expansion of the wave function into plane waves and appropriate regular Monkhorst-Pack  $k$ -point grids were chosen to ensure that all enthalpy calculations were well converged to 1 meV/atom. The *ab initio* molecular dynamics (AIMD) simulations were performed in the canonical ensemble applying a Nosé thermostat. A system containing 128 atoms was used for  $\text{H}_2\text{O}_2$  at 500 GPa. The simulations lasted  $\sim 4ps$  with a time step of 0.5 fs, and a  $1 \times 1 \times 1$   $k$ -mesh grid was used for the Brillouin-zone sampling. Phonon calculations were carried out using the frozen phonon approach as implemented in the PHONOPY package [34]. The

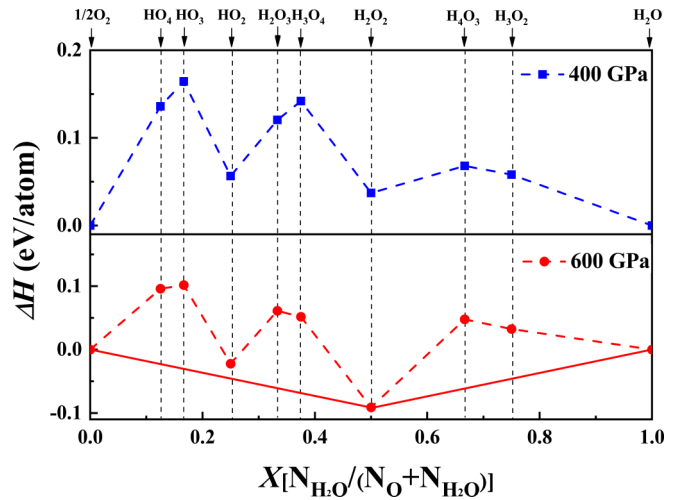


FIG. 1. Phase stabilities of various oxygen-rich H-O compounds with respect to decomposition into solid  $\text{O}_2$  and  $\text{H}_2\text{O}$  at 400 and 600 GPa. The convex hulls are shown with solid lines. Dotted guide-lines directly connect the data points. Compounds corresponding to data points located on the convex hull are thermodynamically stable.

Visualization for Electronic and Structural Analysis software (VESTA 3) was used for visualization and plotting [35].

## III. RESULTS AND DISCUSSION

In order to obtain stable structures for oxygen-rich H-O compounds, the stoichiometries of  $\text{HO}_x$  ( $x = 4, 3, 2, 3/2, 4/2, 1, 3/4, \text{ and } 2/3$ ) with simulation cell size up to four formula units (f.u.) were systematically searched at pressures of 400 and 600 GPa. The thermodynamic stability of different

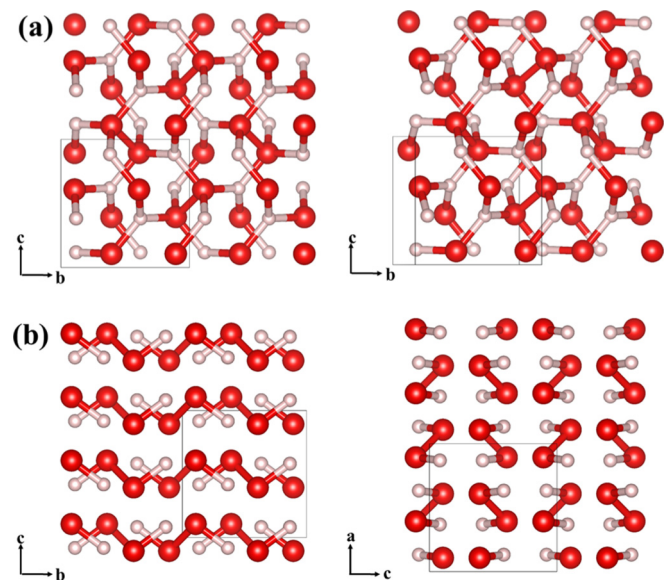


FIG. 2. Stable structures of hydrogen peroxide: (a) the pyrite-type structure with space group of  $Pa-3$  in Ref. [19] and (b) the orthorhombic structure with space group of  $Pbca$  at 500 GPa derived from the CALYPSO structure search. Two sides of views are given. The red and white spheres represent oxygen and hydrogen atoms, respectively.

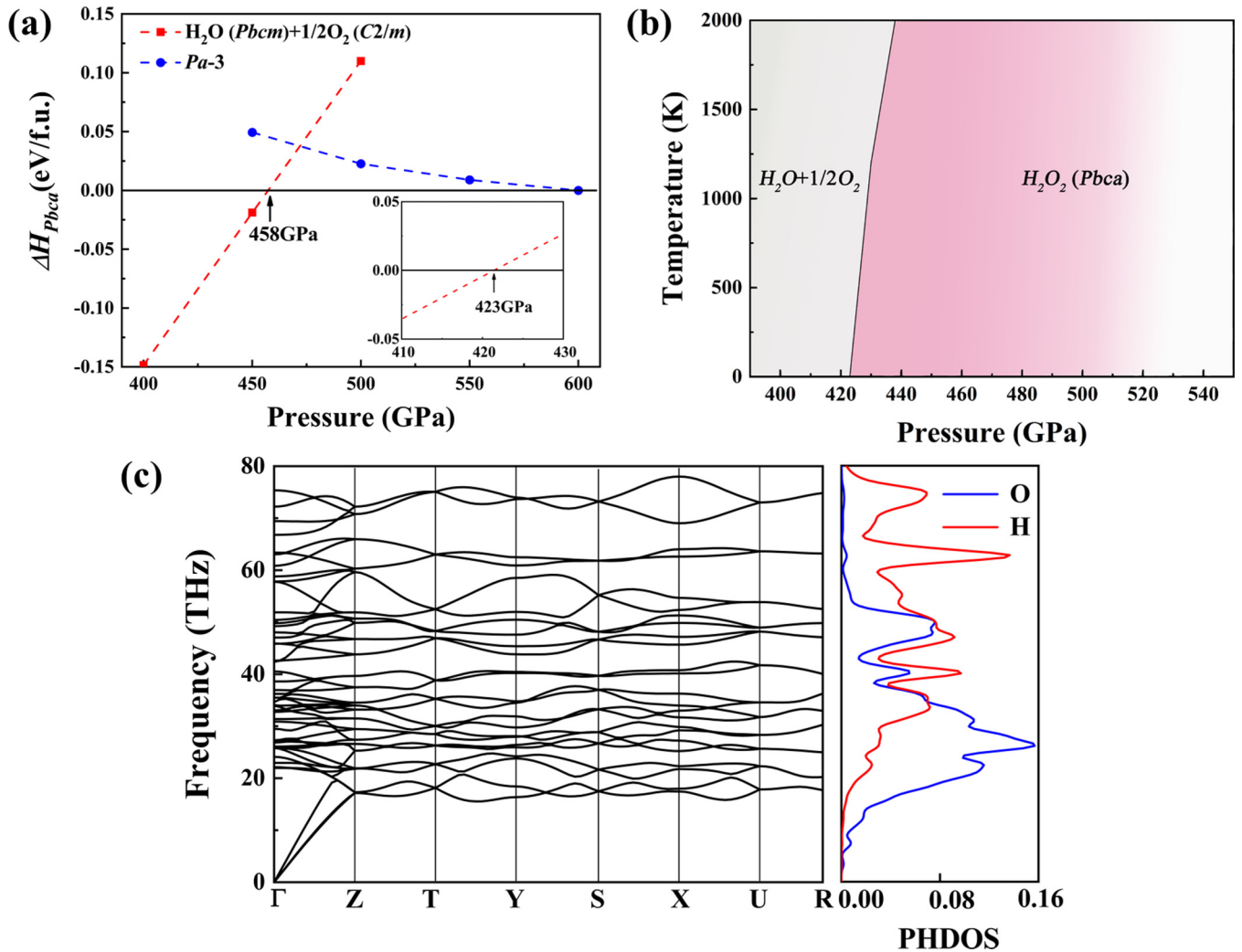


FIG. 3. (a) Calculated enthalpies per formula unit as functions of pressure of different structures relative to the  $Pbcm$  structure without the inclusion of zero-point energy. Inset shows enthalpy curve with inclusion of zero-point energy. (b) Phase diagram of water ice and hydrogen peroxide including vibrational motion. (c) Phonon dispersions of  $Pbcm$  structure of  $\text{H}_2\text{O}_2$  (left panel) at 500 GPa; hydrogen and oxygen projected phonon density of states (right panel). Blue and red lines are the oxygen and hydrogen projected phonon density of states, respectively.

H-O compounds with respect to stable solid  $\text{O}_2$  [36,37] and  $\text{H}_2\text{O}$  [13] at each pressure was evaluated through the below equation:

$$\Delta G_f(\text{HO}_x) = [G(\text{HO}_x) - 1/2G(\text{H}_2\text{O}) - 1/2(x - 1/2)G(\text{O}_2)] / (1 + x), \quad (1)$$

where  $G = U + PV - TS$  is the Gibbs free energy of each composition and  $\Delta G_f$  is the Gibbs free energy of formation per atom. Here,  $U$ ,  $P$ ,  $V$ ,  $T$ , and  $S$  are the internal energy, pressure, volume, temperature, and entropy, respectively. Note that  $G$  reduces to the enthalpy ( $H = U + PV$ ) at  $T = 0$  K. Based on the above definition, the pressure-composition phase diagram at 0 K for  $\text{HO}_x$  systems is shown in Fig. 1, in which the convex hull was constructed by the calculated enthalpies of the most stable structures for each composition. The structure whose formation enthalpy lies on the convex hull (solid lines) is deemed to be stable with respect to decomposition into elements or other compounds, whereas the structure above the convex hull (dotted line) is metastable or

unstable [38]. It is clearly seen from Fig. 1 that all the H-O compounds under consideration are not stable relative to solid  $\text{O}_2$  and  $\text{H}_2\text{O}$  at 400 GPa. This finding is consistent with the common knowledge that  $\text{H}_2\text{O}$  is the only stable compound for H-O system at low pressures. However, further increasing the pressure to 600 GPa, the  $\text{H}_2\text{O}_2$  becomes stable against decomposition into solid  $\text{O}_2$  and  $\text{H}_2\text{O}$ .

At 400 and 600 GPa, our structure searches can readily reproduce the previous pyrite-type  $\text{H}_2\text{O}_2$  structure with space group of  $Pa-3$  [Fig. 2(a)] [19], validating our methodology in application to dense H-O systems. In addition, an orthorhombic  $Pbcm$  structure [Fig. 2(b)] with 4 f.u. per unit cell is found to be more stable than the pyrite-type  $Pa-3$  structure at both pressures. The structural parameters of the new  $Pbcm$  structure at 500 GPa are  $a = 3.328$  Å,  $b = 3.407$  Å,  $c = 3.398$  Å, with H at  $8c$  (0.1347, 0.8680, 0.5822) and O at  $8c$  (0.1072, 0.3926, 0.3939) sites. As depicted in Fig. 2, the predicted orthorhombic  $Pbcm$  structure is a molecular crystal formed through stacking of hydrogen peroxide molecules that is very different from the previous  $Pa-3$  structure occurring

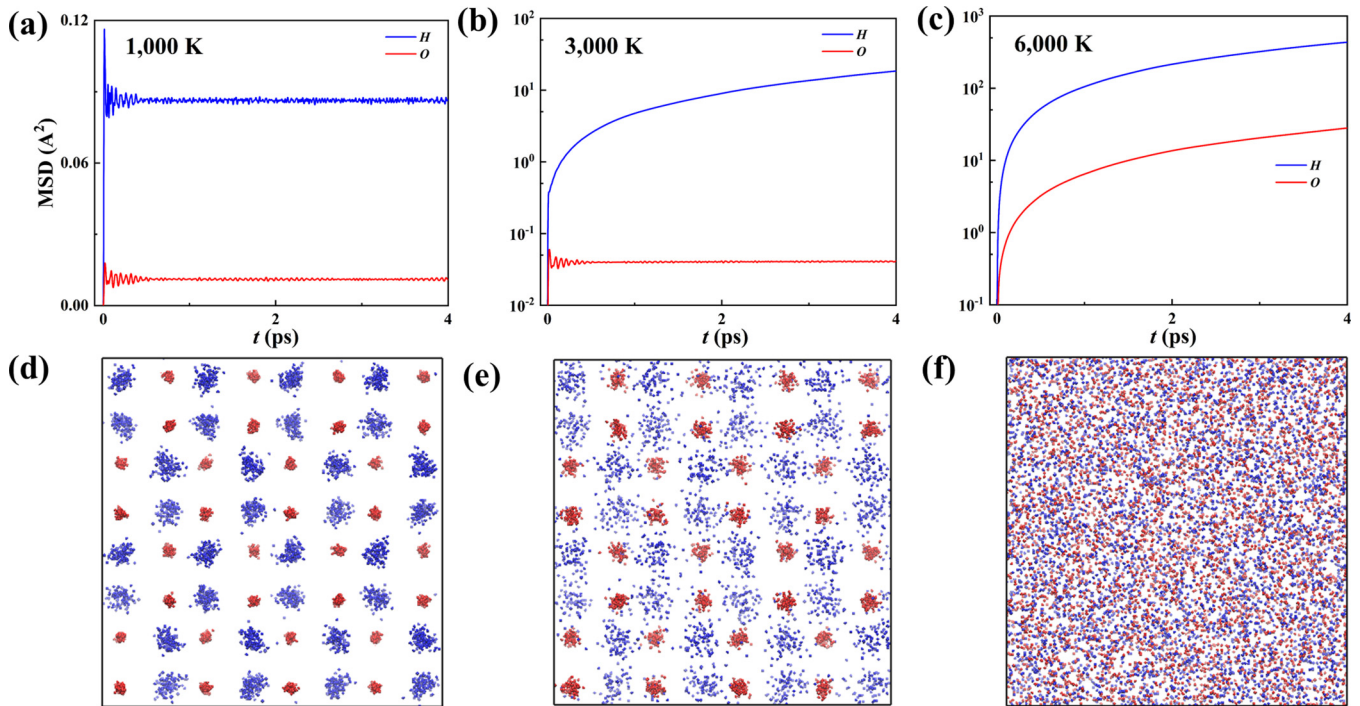


FIG. 4. AIMD simulations of crystalline solid, superionic solid, and fluid phases of  $\text{H}_2\text{O}_2$ . (a)–(c) MSD of oxygen and hydrogen in  $\text{H}_2\text{O}_2$  at (a) 1000 K, (b) 3000 K, and (c) 6000 K at 500 GPa, in three phases. (d)–(f) Trajectory snapshots of the corresponding phases, where the purple and blue spheres represent instantaneous positions of oxygen and hydrogen atoms, respectively.

as an atomic crystal with the hydrogen peroxide unit indiscernible. The coordination environments of the two structures are also different. The O atoms are twofold- and fourfold coordinated in *Pbca* and *Pa-3* structures, while the H atoms are coordinated with one O and three O atoms, respectively. However, both structures contain O–O single bond with length of  $\sim 1.25$  Å at 500 GPa, which is longer than the O–O double bond (1.12 Å) in solid  $\text{O}_2$  at 500 GPa. Interestingly, the hydrogen peroxide molecule in the *Pbca* structure is planar. This is different from the hydrogen peroxide molecule at ambient condition which is nonplanar with dihedral angle of  $90.2^\circ$  due to the electronic repulsion between the lone pairs of the adjacent oxygen atoms [39]. The planarity of hydrogen peroxide molecules in *Pbca* structure is expected to be caused by the steric repulsion between molecules at high pressure. It reduces the steric size of the molecules and leads to a denser packing of the crystal, which lowers the PV term of the enthalpy.

Figure 3(a) shows the calculated static enthalpies of the two high-pressure structures of  $\text{H}_2\text{O}_2$  and their possible decomposition products of solid  $\text{O}_2$  (*C2/m* structure [37]) and  $\text{H}_2\text{O}$  (*Pbcm* structure [13]). We find that the *Pbca* structure becomes stable against decomposition into solid  $\text{O}_2$  and  $\text{H}_2\text{O}$  at pressure about  $\sim 458$  GPa. It has the lowest enthalpy up to  $\sim 600$  GPa, beyond which the *Pa-3* structure is energetically more favorable. It is important to include the quantum nuclear zero-point (ZP) motion when considering the energetics of systems containing light elements. We therefore explored the effect of ZP energy correction within the quasiharmonic approximation and evaluated the corresponding contributions to the free energies. Accordingly, the phase diagram of  $\text{H}_2\text{O}_2$  including vibrational motion up to 2000 K was constructed

[Fig. 3(b)]. The results indicate that the ZP energy further shifts the onset of the stable pressure of *Pbca* structure down to  $\sim 423$  GPa at 0 K [inset in Fig. 3(a)]. Note that the stable field ( $\sim 423$ –600 GPa) of the *Pbca* structure of  $\text{H}_2\text{O}_2$  is much lower than pressure of  $\sim 1$  TPa recently achieved in static compression experiments by a secondary anvil diamond cell [40].

We calculated phonon dispersion curves for the *Pbca* structure at 500 GPa using the supercell method. The absence of any imaginary phonon frequencies in the whole Brillouin zone indicates that the *Pbca* structure is dynamically stable [Fig. 3(c)]. Furthermore, it is clearly seen that the H atom mainly contributes to the high-frequency vibrations because of its relatively lighter atomic mass, while the O atom dominates the low-frequency vibrations.

The stable pressure range ( $\sim 423$ –600 GPa) of the *Pbca* structure has been suggested to occur within some gas giant planets such as Uranus and Neptune [4,13] but accompanied with high temperature of  $\sim 5000$ –6000 K. Therefore, we performed AIMD simulations to consider the high-temperature behavior of this structure. The simulated mean-square displacement (MSD) and trajectory at 500 GPa are presented in Fig. 4. At 1000 K, MSD values of the hydrogen and oxygen atoms remain nearly steady [Fig. 4(a)], indicating that the system is stable in the solid with all atoms close to their equilibrium positions [Fig. 4(d)]. At 3000 K, the hydrogen atom MSD values gradually increase, whereas the oxygen atoms continue to be stable, which represents a transition into a superionic state [Fig. 4(b)]. From the trajectory data, we can easily observe that the oxygen atoms remain near their equilibrium positions while hydrogen atoms diffuse [Fig. 4(e)]. Further increasing the temperature to 6000 K, the

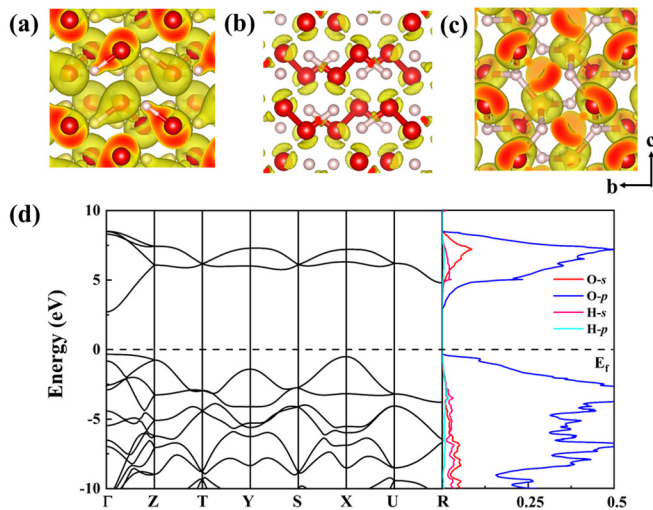


FIG. 5. Isosurfaces of ELF for (a) *Pbc* structure with a value of 0.7, (b) *Pbc* structure with a value of 0.88, (c) *Pa-3* structure with a value of 0.75. (d) Calculated electronic band structures (left panel) and projected density of states (right panel) for *Pbc* structure.

oxygen atoms present a diffusion state, indicative of melting [Figs. 4(c) and 4(f)].

To gain deep insight into the chemical bonding nature of the two high-pressure structures of  $\text{H}_2\text{O}_2$ , we have calculated the electronic localization function (ELF), which, defined to have the convenient range of values between 0 and 1, is known to be an informative tool to distinguish different bonding interactions in molecules or solids [41]. The regions in which the ELF value is close to 0.5 or 1.0 correspond to a perfect free-electron gas distribution or well-localized electrons, respectively. For the *Pbc* structure, the isosurface of ELF with a value of 0.70 [Fig. 5(a)] shows substantial accumulation of electrons around each hydrogen peroxide molecule, denoting strong covalent bonding nature of neighboring O-O and O-H pairs within the molecule; isosurface of ELF with a value of 0.88 [Fig. 5(b)] clearly shows two lone electron pairs on each O atom, which combined with O-O and O-H bonds are distributed tetrahedrally. For the *Pa-3* structure, the ELF plot in Fig. 5(c) indicates that all the neighboring O-O and O-H pairs form covalent bonds, in which each O atom is covalently bonded by three H atoms almost in a plane and by one O atom perpendicular to the  $\text{H}_3\text{O}$  plane.

To quantitatively evaluate the bonding interactions, we also calculated the integrated crystal orbital Hamilton populations (ICOHPs) using the linear muffin-tin orbital method [42].

The ICOHP counts the energy-weighted population of wave functions between two atomic orbitals for a pair of selected atoms, whose value tends to scale with bond strength (metallic or covalent) in compounds. The results are consistent with the above ELF results. At 500 GPa, the ICOHP values for O-O and O-H pairs are  $-13.40$  and  $-6.87$  eV in *Pbc* structure, respectively, while the values are  $-13.62$  and  $-4.47$  eV in *Pa-3* structure. This indicates that the O-H covalent bonds in *Pbc* structure are stronger than those in *Pa-3* structure. Electronic bond structures and density of states for *Pbc* structure at 500 GPa are shown in Fig. 5(d). The *Pbc* structure is insulating with a direct band gap of 3.05 eV at the  $\Gamma$  point of the Brillouin zone. Both valence and conduction bands are dominated by the O  $2p$  states.

#### IV. CONCLUSIONS

In summary, by means of first-principles calculations and the swarm-intelligence structure search method, we identified an orthorhombic phase of  $\text{H}_2\text{O}_2$  with space group of *Pbc* stabilized in pressure range of  $\sim 423$ – $600$  GPa. The structure of the phase is formed by stacking of intriguing planar  $\text{H}_2\text{O}_2$  molecules. The planarity of the  $\text{H}_2\text{O}_2$  molecule is caused by the steric repulsion between molecules at high pressure, which reduces the steric size of the molecules and leads to a denser packing of the crystal, responsible for the stability of the structure. The phase is thus a low-pressure phase of the binary H-O system with H:O stoichiometry other than 2:1, and its stable field is promising to be accessible in current static compression experiment using diamond-anvil cell. The stable pressure range ( $\sim 423$ – $600$  GPa) of the  $\text{H}_2\text{O}_2$  phase has been suggested to occur within some gas giant planets such as Uranus and Neptune [4,13] but accompanied with high temperature of  $\sim 5000$ – $6000$  K. At these P-T conditions,  $\text{H}_2\text{O}_2$  should exist in the form of fluid according to the AIMD simulations. The current results will inevitably advance our understanding of the high-pressure behavior of the binary H-O system.

#### ACKNOWLEDGMENTS

The authors acknowledge the funding support from Jilin Province Outstanding Young Talents Project No. 20190103040JH), National Natural Science Foundation of China (Grants No. 11974134, No. 11534003, No. 11404128, No. 11822404, and No. 11904129), and the Science Challenge Project No. TZ2016001. Part of the calculations were performed in the high-performance computing center of Jilin University and Tianhe2-JK in the Beijing Computational Science Research Center.

[1] W.B. Hubbard, *Planetary Interiors* (Van Nostrand Reinhold, New York, 1984).  
 [2] D. Arnett, *Supernovae and Nucleosynthesis* (Princeton University, Princeton, NJ, 1996).  
 [3] T. Guillot, *Science* **286**, 72 (1999).  
 [4] B. Militzer, W. B. Hubbard, J. Vorberger, I. Tamblyn, and S. A. Boney, *Astrophys. J.* **688**, L45 (2008).

[5] V.F. Petrenko and R.W. Whitworth, *Physics of Ice* (Oxford University Press, Oxford, 2002).  
 [6] C. G. Salzmann, P. G. Radaelli, E. Mayer, and J. L. Finney, *Phys. Rev. Lett.* **103**, 105701 (2009).  
 [7] A. Polian and M. Grimsditch, *Phys. Rev. Lett.* **52**, 1312 (1984).  
 [8] A. F. Goncharov, V. V. Struzhkin, M. S. Somayazulu, R. J. Hemley, and H. K. Mao, *Science* **273**, 218 (1996).

- [9] J.-P. Davis, C. Deeney, M. D. Knudson, R. W. Lemke, T. D. Pointon, and D. E. Bliss, *Phys. Plasmas* **12**, 056310 (2005).
- [10] D. H. Dolan, M. D. Knudson, C. A. Hall, and C. Deeney, *Nat. Phys.* **3**, 339 (2007).
- [11] K. K. M. Lee, L. R. Benedetti, R. Jeanloz, P. M. Celliers, J. H. Eggert, D. G. Hicks, S. J. Moon, A. Mackinnon, L. B. Da Silva, D. K. Bradley, W. Unites, G. W. Collins, E. Henry, M. Koenig, A. Benuzzi-Mounaix, J. Pasley, and D. Neely, *J. Chem. Phys.* **125**, 014701 (2006).
- [12] M. Benoit, M. Bernasconi, P. Focher, and M. Parrinello, *Phys. Rev. Lett.* **76**, 2934 (1996).
- [13] B. Militzer and H. F. Wilson, *Phys. Rev. Lett.* **105**, 195701 (2010).
- [14] Y. Wang, H. Liu, J. Lv, L. Zhu, H. Wang, and Y. Ma, *Nat. Commun.* **2**, 563 (2011).
- [15] J. M. McMahon, *Phys. Rev. B* **84**, 220104(R) (2011).
- [16] M. Ji, K. Umemoto, C.-Z. Wang, K.-M. Ho, and R. M. Wentzcovitch, *Phys. Rev. B* **84**, 220105(R) (2011).
- [17] A. Hermann, N. W. Ashcroft, and R. Hoffmann, *Proc. Natl. Acad. Sci. USA* **109**, 745 (2012).
- [18] S. Zhang, H. F. Wilson, K. P. Driver, and B. Militzer, *Phys. Rev. B* **87**, 024112 (2013).
- [19] C. J. Pickard, M. Martinez-Canales, and R. J. Needs, *Phys. Rev. Lett.* **110**, 245701 (2013).
- [20] P. Huang, H. Liu, J. Lv, Q. Li, C. Long, Y. Wang, C. Chen, R. J. Hemley, and Y. Ma, *Proc. Natl. Acad. Sci. USA* **117**, 5638 (2020).
- [21] H. F. Wilson and B. Militzer, *Astrophys. J.* **745**, 54 (2012).
- [22] Y. Wang, J. Lv, L. Zhu, and Y. Ma, *Phys. Rev. B* **82**, 094116 (2010).
- [23] Y. Wang, J. Lv, L. Zhu, and Y. Ma, *Comput. Phys. Commun.* **183**, 2063 (2012).
- [24] J. Lv, Y. Wang, L. Zhu, and Y. Ma, *Phys. Rev. Lett.* **106**, 015503 (2011).
- [25] L. Zhu, H. Wang, Y. Wang, J. Lv, Y. Ma, Q. Cui, Y. Ma, and G. Zou, *Phys. Rev. Lett.* **106**, 145501 (2011).
- [26] L. Zhu, H. Liu, C. J. Pickard, G. Zou, and Y. Ma, *Nat. Chem.* **6**, 644 (2014).
- [27] Y. Li, J. Hao, H. Liu, Y. Li, and Y. Ma, *J. Chem. Phys.* **140**, 174712 (2014).
- [28] H. Wang, J. S. Tse, K. Tanaka, T. Iitaka, and Y. Ma, *Proc. Natl. Acad. Sci. USA* **109**, 6463 (2012).
- [29] Y. Li, X. Feng, H. Liu, J. Hao, S. A. T. Redfern, W. Lei, D. Liu, and Y. Ma, *Nat. Commun.* **9**, 722 (2018).
- [30] F. Peng, Y. Sun, C. J. Pickard, R. J. Needs, Q. Wu, and Y. Ma, *Phys. Rev. Lett.* **119**, 107001 (2017).
- [31] G. Kresse and J. Furthmüller, *Phys. Rev. B* **54**, 11169 (1996).
- [32] P. E. Blöchl, *Phys. Rev. B* **50**, 17953 (1994).
- [33] J. P. Perdew, K. Burke, and M. Ernzerhof, *Phys. Rev. Lett.* **77**, 3865 (1996).
- [34] A. Togo and I. Tanaka, *Scr. Mater.* **108**, 1 (2015).
- [35] K. Momma and F. Izumi, *J. Appl. Crystallogr.* **44**, 1272 (2011).
- [36] Y. Akahama, H. Kawamura, D. Häusermann, M. Hanfland, and O. Shimomura, *Phys. Rev. Lett.* **74**, 4690 (1995).
- [37] Y. Ma, A. R. Oganov, and C. W. Glass, *Phys. Rev. B* **76**, 064101 (2007).
- [38] X. Zhang, G. Trimarchi, and A. Zunger, *Phys. Rev. B* **79**, 092102 (2009).
- [39] W. R. Busing and H. A. Levy, *J. Chem. Phys.* **42**, 3054 (1965).
- [40] N. Dubrovinskaia, L. Dubrovinsky, N. A. Solopova, A. Abakumov, S. Turner, M. Hanfland, E. Bykova, M. Bykov, C. Prescher, V. B. Prakapenka, S. Petitgirard, I. Chuvashova, B. Gasharova, Y.-L. Mathis, P. Ershov, I. Snigireva, and A. Snigirev, *Sci. Adv.* **2**, e1600341 (2016).
- [41] A. D. Becke and K. E. Edgecombe, *J. Chem. Phys.* **92**, 5397 (1990).
- [42] R. Dronskowski and P. E. Bloechl, *J. Phys. Chem.* **97**, 8617 (1993).